Enhancing Mendelian Randomization Causal Inference through Pleiotropic Clustering in the Presence of Correlated Horizontal Pleiotropy

Supplementary Tables

Supplementary Table 1: False positive rate or Power to detect correlated horizontal pleiotropy in MR for different methods

Correlated horizontal pleiotropy	Uncorrelated horizontal pleiotropy	P-threshold	Methods	Causal effect/Correlated horizontal pleiotropic effect (γ/η)						
				$\sqrt{0.00}$	$\sqrt{0.01}$	$\sqrt{0.02}$	$\sqrt{0.03}$	$\sqrt{0.04}$	$\sqrt{0.05}$	mean(%)
The Null (Absence)	Absence	0.05	MR-PRESSO	5	5	4	5	5	2	4.33
		0.05	PCMR	5	1	7	7	4	5	4.83
		0.10	MR-PRESSO	14	13	8	13	10	8	11.00
		0.10	PCMR	11	7	10	12	13	10	10.50
	Presence	0.05	MR-PRESSO	51	49	46	49	41	52	48.00
		0.05	PCMR	6	7	4	8	7	2	5.67
		0.10	MR-PRESSO	54	58	54	57	53	61	56.17
		0.10	PCMR	9	11	8	12	13	5	9.67
The Alternative (Presence)	Absence	0.05	MR-PRESSO	-	17	40	58	76	77	Δ6.00
		0.05	PCMR	-	10	30	57	67	74	
		0.10	MR-PRESSO	-	26	52	74	85	90	Δ6.20
		0.10	PCMR	-	24	41	67	82	82	
	Presence	0.05	MR-PRESSO	-	68	75	81	94	93	-
		0.05	PCMR	-	13	26	33	51	63	-
		0.10	MR-PRESSO	-	77	84	87	97	97	-
		0.10	PCMR	-	23	35	47	62	72	-

Power (%). There are 100 simulations in each scenario. In the absence of correlated horizontal pleiotropy (The Null), the scenarios are simulated in causal effects, γ, from $\sqrt{0.00}$ to $\sqrt{0.05}$. In the presence of correlated horizontal pleiotropy (The Alternative), the scenarios set the causal effect at zero and simulated in 40% correlated horizontal pleiotropic variants with effect η from $\sqrt{0.01}$ to $\sqrt{0.05}$. The heritability of exposure is solely through exposure or confounding in the absence of uncorrelated horizontal pleiotropy, or set at 0.25 in the presence of correlated horizontal pleiotropy. The Δ-mean indicates the mean power difference between MR-PRESSO and PCMR's pleiotropy test.

Supplementary Table 2: The GWAS summary statistics for Common diseases and psychiatric disorders.

Trait	Abbreviation	Sample Size	PMID	First Author(Year)
Triglycerides[1]	tg	188577	24097068	Willer (2013)
ldl[1]	ldl	188577	24097068	Willer (2013)
hdl[1]	hdl	188577	24097068	Willer (2013)
height[2]	height	456426	30124842	Yengo L(2018)
body mass index[3]	bmi	238944	25673413	Locke AE (2015)
body fat percentage[4]	bf	100716	26833246	Lu Y (2016)
birth weight[5]	bw	133903	27680694	Horikoshi M (2016)
diastolic blood pressure[6]	dbp	757601	30224653	Evangelou E (2018)
systolic blood pressure[6]	sbp	757601	30224653	Evangelou E (2018)
fasting blood glucose[7]	fg	46186	20081858	Dupuis J (2010)
ever regular smoker[8]	smoking	1232091	30643251	Liu M (2019)
drinks per week[8]	alcohol	941280	30643251	Liu M (2019)
coronary artery disease[9]	cad	547261	29212778	van der Harst P (2017)
any stroke[10]	stroke	446696	29531354	Malik R (2018)
type 2 diabetes[11]	t2d	69033	22885922	Morris AP (2012)
asthma[12]	asthma	127669	29273806	Demenais F (2017)
Schizophrenia[13]	scz	144605	35396580	Trubetskoy V(2022)
Major depressive disorder[14]	mdd	170756	30718901	Howard(2019)
Type 1 bipolar disorder[15]	bip1	475038	34002096	Mullins(2021)

Supplementary Figures

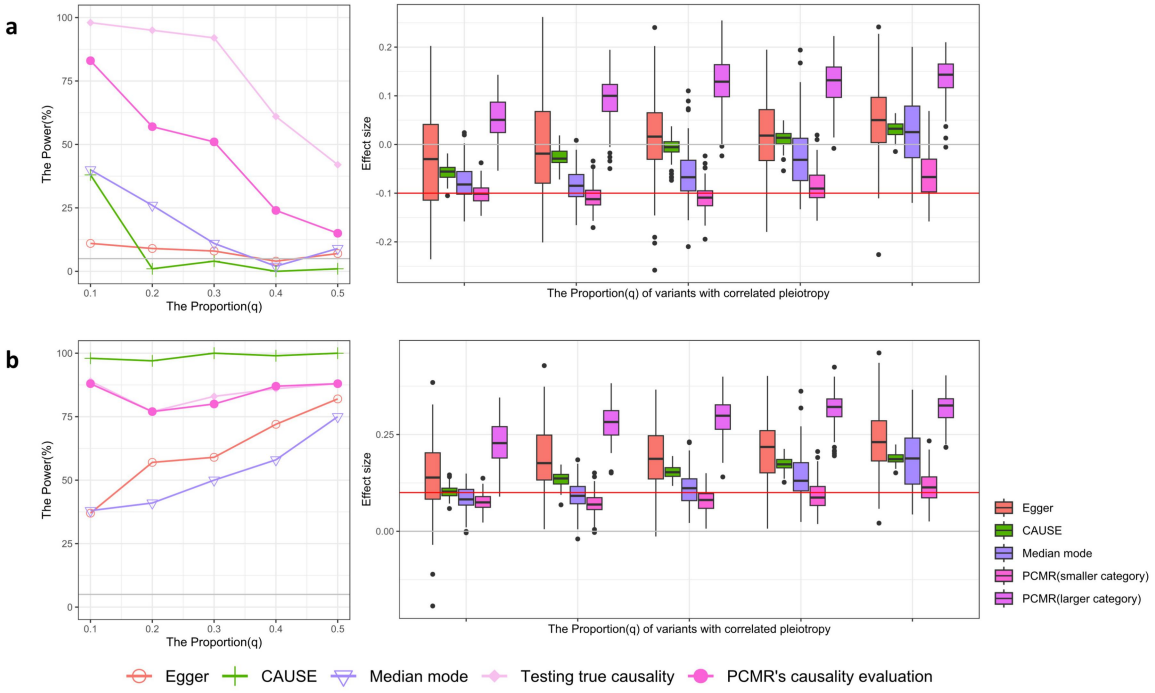

Supplementary Fig. 1| The power and estimates of PCMR and three alternative MR methods in alternative hypothesis with correlated horizontal pleiotropy. a, Comparison when causal effect ($\gamma = -0.1$) and correlated horizontal pleiotropic effect in opposite. The proportion of correlated horizontal pleiotropic variants is from 10% to 50%, and the heritability of outcomes mediated by causal effects and confounding is 5%. **b,** Comparison when causal effect ($\gamma = 0.1$) and correlated horizontal pleiotropic effect in the same direction. Testing true causality indicates that when the IV category determining true causal effect is identified, causal inference for this IV category relies on bootstrapping. There are 100 simulations in each scenario using a p-value threshold of 0.05.

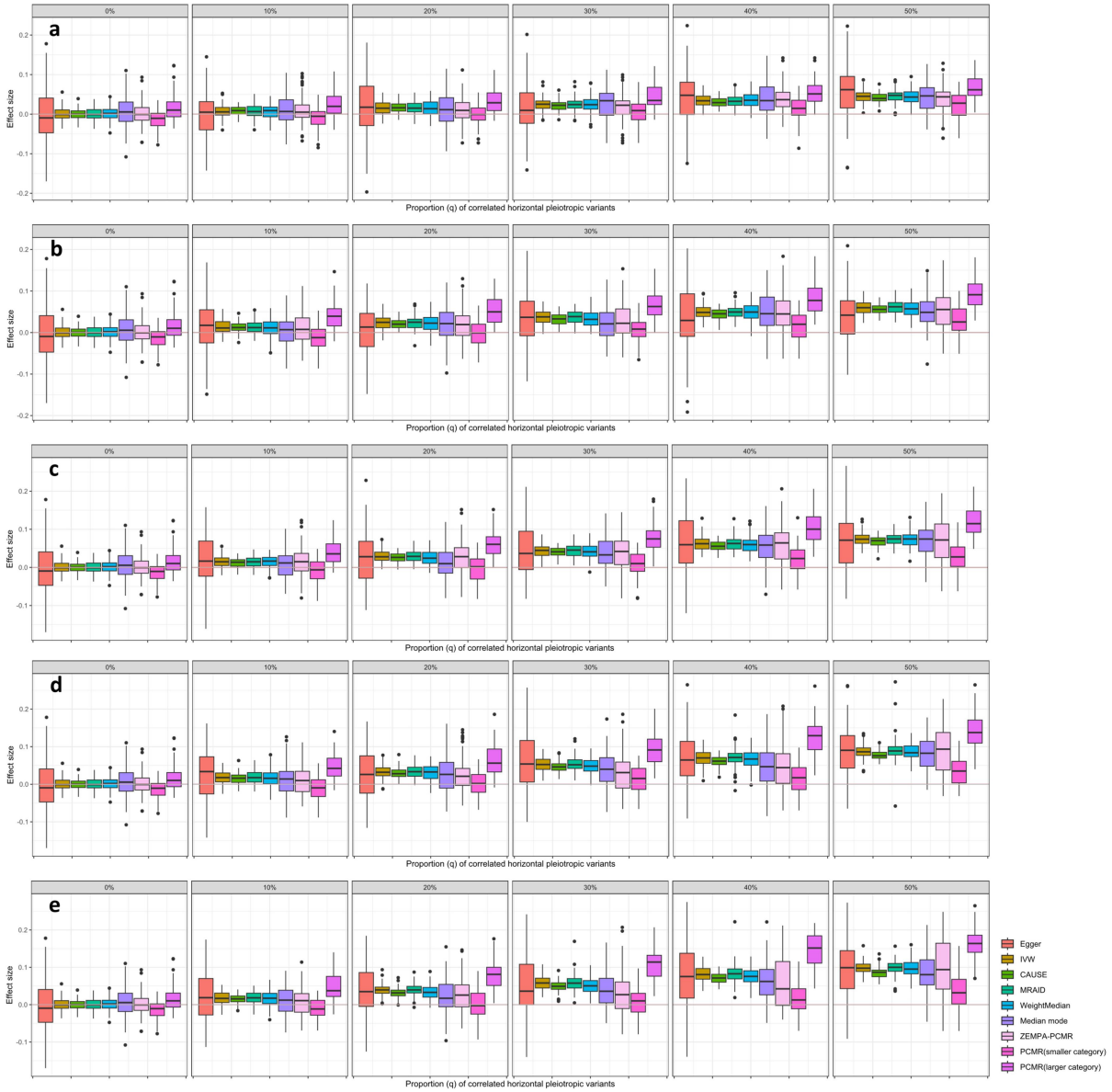

Supplementary Fig. 2| The random effect model of PCMR and alternative methods in the null hypothesis. The actual causal effect is zero in the presence of correlated pleiotropic variants ranging from 0% to 50% and correlated horizontal pleiotropic effects from $\sqrt{0.01}$ to $\sqrt{0.05}$. **a,** $\eta = \sqrt{0.01}$ **b,** $\eta = \sqrt{0.02}$ **c**, $\eta = \sqrt{0.03}$ **d**, $\eta = \sqrt{0.04}$ **e**, $\eta = \sqrt{0.05}$

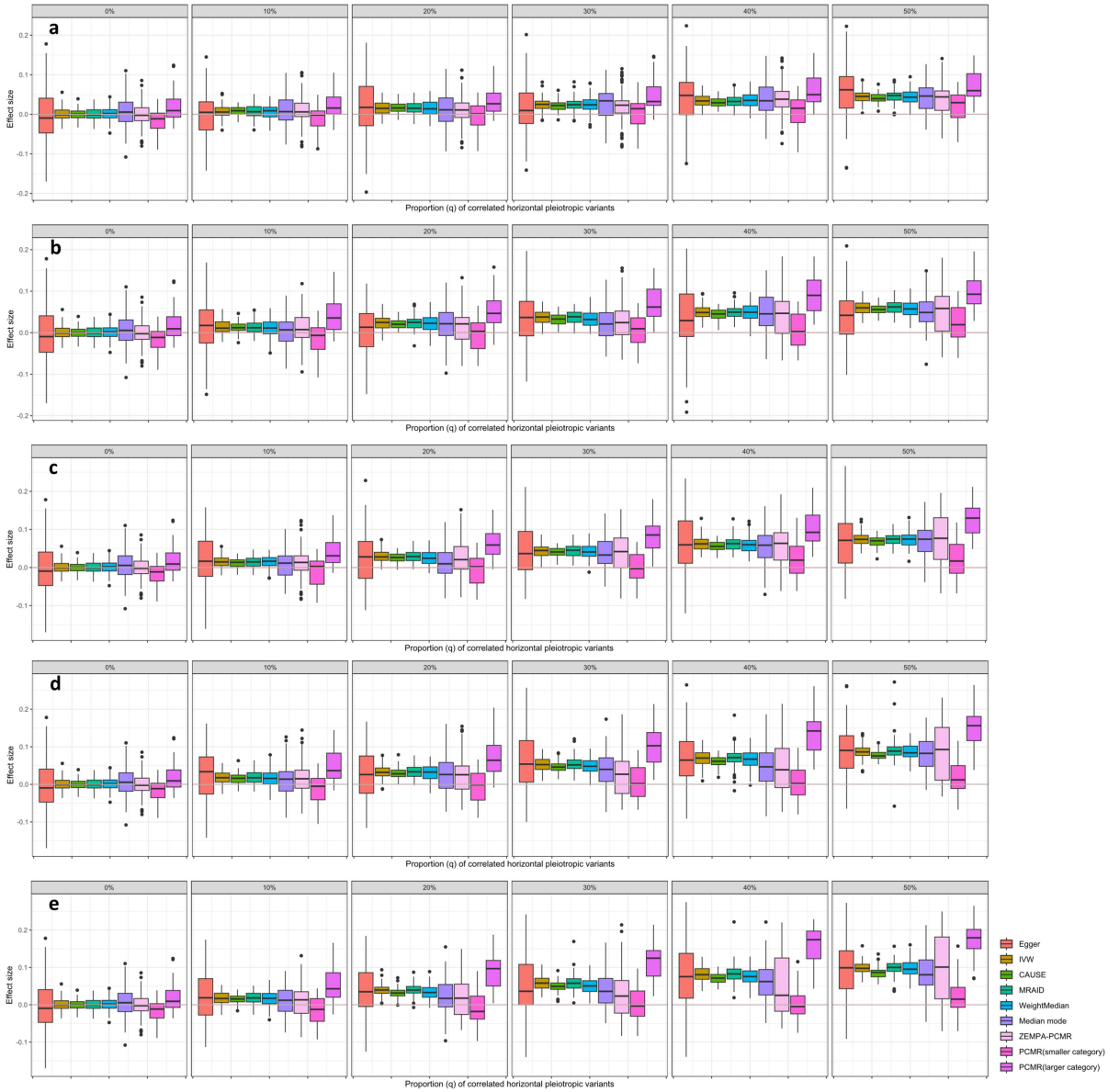

Supplementary Fig. 3| The fixed effect model of PCMR and alternative methods in the null hypothesis. The actual causal effect is zero in the presence of correlated pleiotropic variants ranging from 0% to 50% and correlated horizontal pleiotropic effects from $\sqrt{0.01}$ to $\sqrt{0.05}$. **a,** $\eta = \sqrt{0.01}$ **b,** $\eta = \sqrt{0.02}$ **c**, $\eta = \sqrt{0.03}$ **d**, $\eta = \sqrt{0.04}$ **e**, $\eta = \sqrt{0.05}$

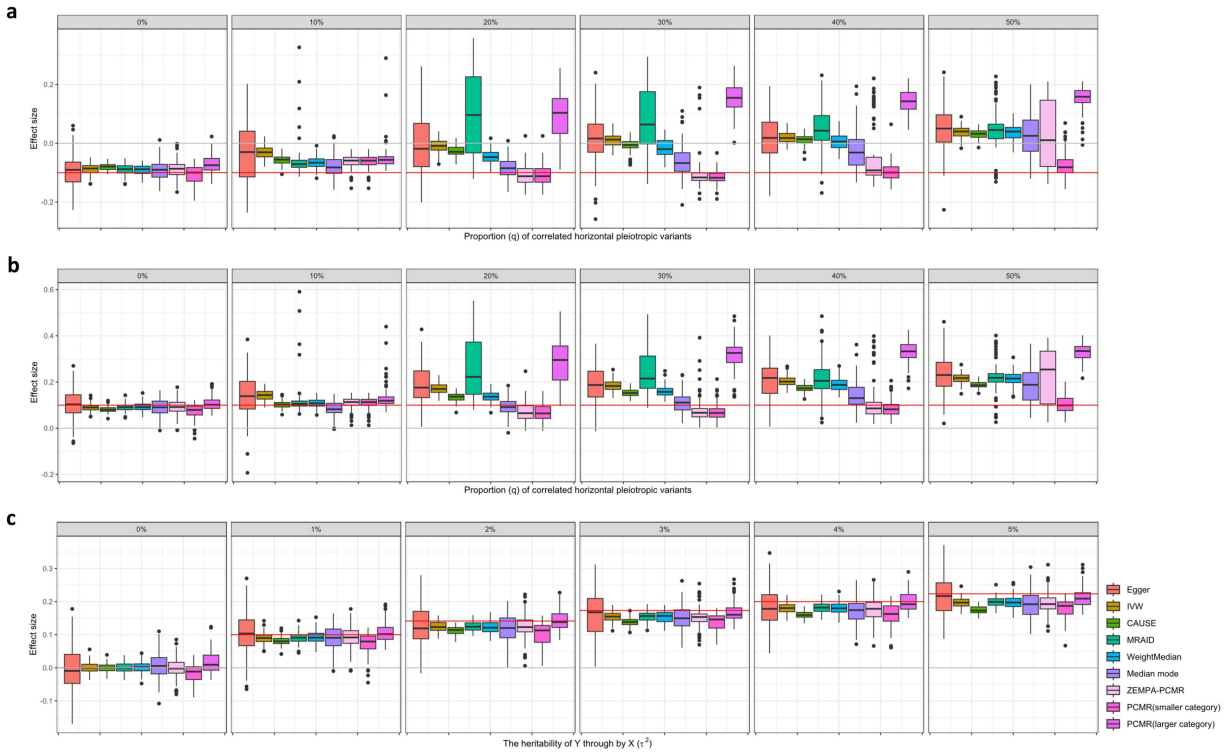

Supplementary Fig. 4| The fixed effect model of PCMR and other MR methods in the alternative hypothesis. a, b, c, Box plot of estimated causal effect by methods. a, b, Comparison of estimated effect in the presence of correlated pleiotropy. The proportion of correlated horizontal pleiotropic variants from 0% to 50%, and the heritability of outcome mediated by exposure and confounding, $\tau^2 + \omega^2$, is 5%. **a**, $\gamma = -0.1$ is in the opposite direction with correlated horizontal pleiotropic effect ($\eta = \sqrt{\omega^2}$); **b**, $\gamma = 0.1$ is the same direction with correlated horizontal pleiotropic effect. **c**, Comparison of estimated effect in the absence of correlated pleiotropy. The heritability of outcome mediated by exposure, τ^2, from 1% to 5%. ($\gamma = \sqrt{\tau^2}$)

a

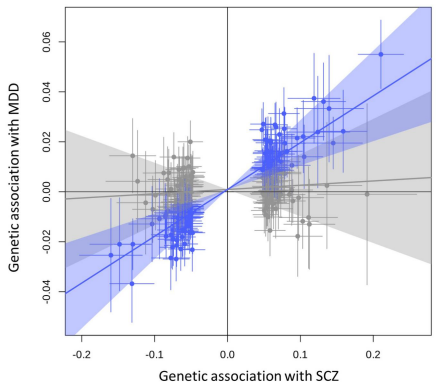

BLUE Category	GRAY Category
chemical synaptic transmission	0.000587898
anterograde trans-synaptic signaling	0.000587898
trans-synaptic signaling	0.000653191
cell-cell signaling	0.00065642
synaptic signaling	0.000902912
postsynaptic modulation of chemical synaptic transmission	0.003077533
modulation of chemical synaptic transmission	0.003645792
regulation of trans-synaptic signaling	0.003712838
regulation of biological quality	0.004674875
...	...

b

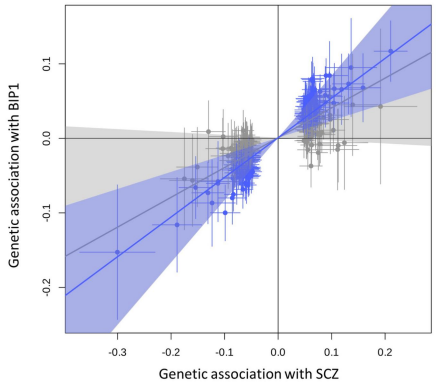

BLUE Category	GRAY Category
regulation of synaptic plasticity	0.000105586
modulation of chemical synaptic transmission	0.000285301
regulation of trans-synaptic signaling	0.000291633
regulation of cellular process	0.000383319
chemical synaptic transmission	0.000675584
anterograde trans-synaptic signaling	0.000675584
trans-synaptic signaling	0.000755266
synaptic signaling	0.001063869
cell-cell signaling	0.002352628
...	...

Supplementary Fig. 5| Enrichment analysis based on classified IV categories by PCMR when SCZ is the exposure. The BLUE IV category is the largest proportion. **a**, **SCZ on MDD**. PCMR classified IVs into the BLUE IV category ($\phi_1 = 0.187,\ \sigma^2_{\phi_1} = 0.002,\ 50.19\%$) and the GRAY IV category ($\phi_2 = 0.017,\ \sigma^2_{\phi_2} = 0.004,\ 49.81\%$). **b**, **SCZ on BIP1.** PCMR classified IVs into the BLUE IV category ($\phi_1 = 0.532,\ \sigma^2_{\phi_1} = 0.024,\ 50.01\%$) and the GRAY IV category ($\phi_2 = 0.399,\ \sigma^2_{\phi_2} = 0.049,\ 49.99\%$).

a

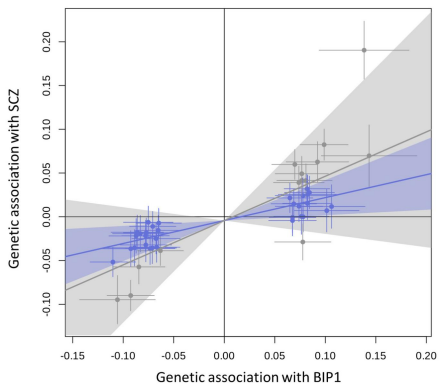

BLUE Category	GRAY Category	
None biological process	membrane depolarization during cardiac muscle cell action potential	8.45148E-05
	membrane depolarization during action potential	0.000414661
	membrane depolarization during atrial cardiac muscle cell action potential	0.000576929
	membrane depolarization during AV node cell action potential	0.001922247
	cardiac muscle cell action potential	0.004072902
	membrane depolarization	0.005554739
	AV node cell to bundle of His cell signaling	0.008640554
	AV node cell action potential	0.008640554
	AV node cell to bundle of His cell communication	0.012667209
	...	...

b

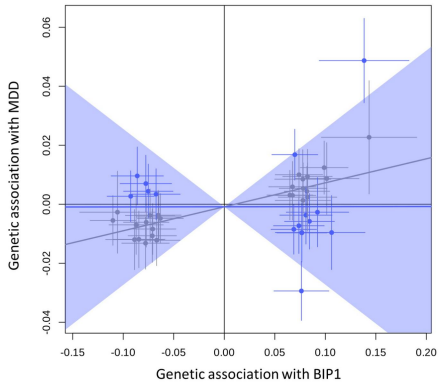

BLUE Category	GRAY Category	
None biological process	membrane depolarization during cardiac muscle cell action potential	0.001105937
	membrane depolarization during atrial cardiac muscle cell action potential	0.003321051
	membrane depolarization during action potential	0.005401904
	membrane depolarization during AV node cell action potential	0.011058986
	AV node cell action potential	0.049639839
	AV node cell to bundle of His cell signaling	0.049639839

Supplementary Fig. 6| Enrichment analysis based on classified IV categories by PCMR when BIP1 is the exposure. The BLUE IV category is the largest proportion. **a**, **BIP1 on SCZ**. PCMR classified IVs into the BLUE IV category ($\phi_1 = 0.262$, $\sigma^2_{\phi_1} = 0.010$, 50.87%) and the GRAY IV category ($\phi_2 = 0.506$, $\sigma^2_{\phi_2} = 0.113$, 49.12%). **b**, **BIP1 on MDD.** PCMR classified IVs into the BLUE IV category ($\phi_1 = 0.000$, $\sigma^2_{\phi_1} = 0.018$, 52.04%) and the GRAY IV category ($\phi_2 = 0.081$, $\sigma^2_{\phi_2} = 0.000$, 47.96%).

a

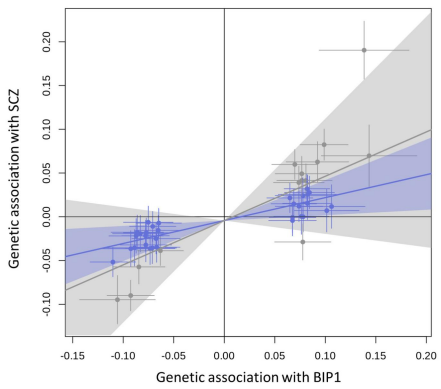

BLUE Category	GRAY Category	
None biological process	membrane depolarization during cardiac muscle cell action potential	8.45148E-05
	membrane depolarization during action potential	0.000414661
	membrane depolarization during atrial cardiac muscle cell action potential	0.000576929
	membrane depolarization during AV node cell action potential	0.001922247
	cardiac muscle cell action potential	0.004072902
	membrane depolarization	0.005554739
	AV node cell to bundle of His cell signaling	0.008640554
	AV node cell action potential	0.008640554
	AV node cell to bundle of His cell communication	0.012667209
	...	...

b

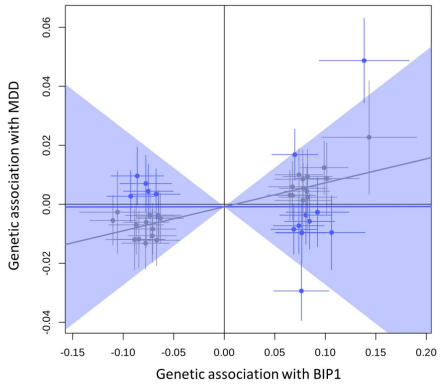

BLUE Category	GRAY Category	
None biological process	membrane depolarization during cardiac muscle cell action potential	0.001105937
	membrane depolarization during atrial cardiac muscle cell action potential	0.003321051
	membrane depolarization during action potential	0.005401904
	membrane depolarization during AV node cell action potential	0.011058986
	AV node cell action potential	0.049639839
	AV node cell to bundle of His cell signaling	0.049639839

Supplementary Fig. 7| Enrichment analysis based on classified IV categories by PCMR when BIP1 is the exposure. The BLUE IV category is the largest proportion. **a**, **BIP1 on SCZ**. PCMR classified IVs into the BLUE IV category ($\phi_1 = 0.262$, $\sigma^2_{\phi_1} = 0.010$, 50.87%) and the GRAY IV category ($\phi_2 = 0.506$, $\sigma^2_{\phi_2} = 0.113$, 49.12%). **b**, **BIP1 on MDD.** PCMR classified IVs into the BLUE IV category ($\phi_1 = 0.000$, $\sigma^2_{\phi_1} = 0.018$, 52.04%) and the GRAY IV category ($\phi_2 = 0.081$, $\sigma^2_{\phi_2} = 0.000$, 47.96%).

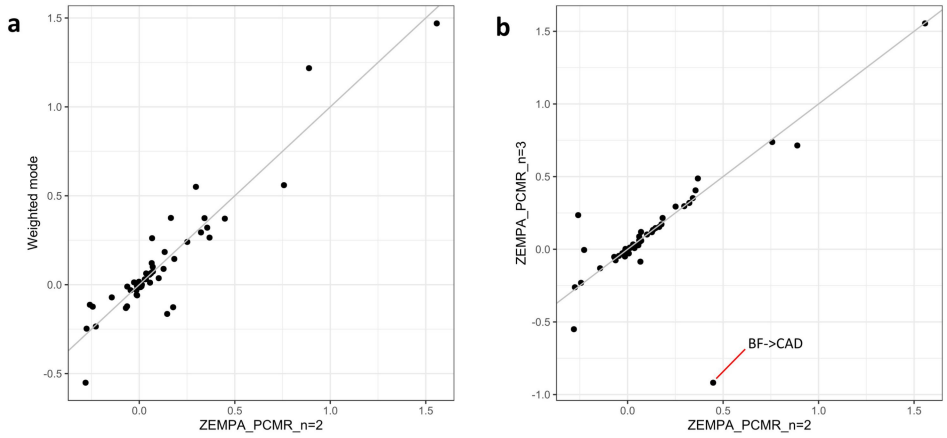

Supplementary Fig. 8| Comparison of PCMR and Weighted mode under the ZEMPA in 48 pairs of common diseases. a, PCMR($n_\phi = 2$) and Weighted mode based on ZEMPA. The correlation coefficient of the estimated results between PCMR($n_\phi = 2$) and Weighted mode reached 0.934. **b**, PCMR($n_\phi = 2$) and PCMR($n_\phi = 3$) based on ZEMPA. Most of the estimates are similar in PCMR($n_\phi = 2$) and PCMR($n_\phi = 3$). For the outlier trait pair, BF and CAD, it is mainly due to the detection of distinct IV categories by ZEMPA. The clustering results of the two models are still similar. (PCMR($n_\phi = 2$): $\phi_1 = 0.448, \phi_2 = -0.665$; PCMR($n_\phi = 3$): $\phi_1 = -0.918, \phi_2 = 0.383, \phi_3 = 0.383$)

SN 1 Discuss negative causal relationships

SN1.1 FG and T2D

According to the categorization of causality credibility in CAUSE, some literature supports the relationship between FG and T2D, yet PCMR's causality evaluation did not yield a significant outcome. To gain a deeper understanding of these findings, we analyzed IVs associated with this pair of traits and attempted to prioritize the IV category determining causality.

PCMR classified the IVs into two distinct categories with correlated horizontal pleiotropic effects: $\phi_1 = 0.166$ ($\sigma^2_{\phi_1} = 0.069, 52.00\%$) and $\phi_2 = 2.075$ ($\sigma^2_{\phi_2} = 0.018, 48.00\%$), respectively. The non-significant result in PCMR's causality evaluation is the absence of a dominant IV category supporting a significant non-zero causal effect. That is attributed to the larger IV category, which contributes to an insignificant non-zero effect ($\phi_1 = 0.166$; a bootstrapping test for this IV category yielded $P_{boot} = 0.398$). Furthermore, we conducted an enrichment analysis of biological processes among the genes mapped by different IV categories, as illustrated in SN Fig. 1a. The enrichment revealed that the BLUE IV category (corresponding to ϕ_1) did not exhibit enrichment in any biological process. Conversely, the GRAY IV category (corresponding to ϕ_2) showed significant enrichment in 48 biological processes, with the regulation of insulin secretion being the most prominent ($P = 5.603 \times 10^{-5}$). Given the importance of insulin regulation in T2D, the GRAY category might exhibit correlated horizontal pleiotropy ($\phi_2 = \gamma + \eta$). Thus, the BLUE category is more likely to correspond to the causality of FG and T2D, and we conducted a bootstrap test to make causal inferences based on the GRAY category ($P_{gray} = 0.398, 95\% CL: (-0.251, 1.761)$). This finding aligns with that of Merino et al.[16], which excludes FG-increasing variants associated with type 2 diabetes.

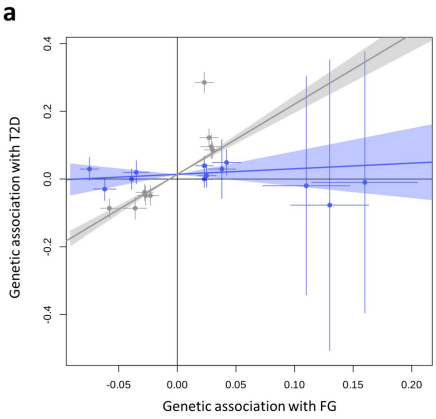

BLUE Category	GRAY Category	
None biological process	regulation of insulin secretion	6.32E-08
	regulation of peptide hormone secretion	9.49E-08
	response to hexose	2.48E-07
	insulin secretion	2.48E-07
	regulation of peptide secretion	5.83E-07
	regulation of peptide transport	9.46E-07
	response to monosaccharide	9.46E-07
	response to carbohydrate	1.08301E-06
	peptide hormone secretion	1.33368E-06
	...	...

BLUE Category		GRAY Category	
neuron development	0.000191147	cell-cell adhesion via plasma-membrane adhesion molecules	0.001125513
plasma membrane bounded cell projection organization	0.00039372	cell-cell adhesion	0.011264522
cell projection organization	0.000513787	cell adhesion	0.046326099
neurogenesis	0.001228196		
neuron differentiation	0.001620562		
nervous system development	0.00190071		
generation of neurons	0.002667066		
cell projection morphogenesis	0.003274217		
cell part morphogenesis	0.004075698		
...	...		

SN Fig. 1|Enrichment analysis based on classified IV categories by PCMR. β_X estimates from GWAS summary of exposure (horizontal axis) are plotted against β_Y estimates from GWAS summary of outcome (vertical axis). **a**, **FG and T2D**. PCMR classified IVs into the BLUE IV category ($\phi_1 = 0.166, \sigma^2_{\phi_1} = 0.069, 52.00\%$) and GRAY IV category ($\phi_2 = 2.075, \sigma^2_{\phi_2} = 0.018, 48.00\%$). **b**, **Smoking and T2D.** PCMR classified IVs into the BLUE IV category ($\phi_1 = -0.063, \sigma^2_{\phi_1} = 0.0, 50.11\%$) and GRAY IV category ($\phi_2 = 0.545, \sigma^2_{\phi_2} = 0.407, 49.89\%$).

SN1.2 Smoking and T2D

Smoking has been identified as a cause of the increased risk of T2D[17], but no method can detect a significant relationship between smoking and T2D. PCMR classified all IVs into two distinct IV categories with correlated HVP effects (proportion) $\phi_1 = -0.063$ ($\sigma^2_{\phi_1} = 0.0, 50.11\%$) and $\phi_2 = 0.545$ ($\sigma^2_{\phi_2} = 0.407, 49.89\%$), respectively. Though PCMR's pleiotropy test did not detect significant correlated horizontal pleiotropy ($P_{plei-test} = 0.269$), the two IV categories showed distinct associated biological processes in enrichment analysis, as shown in SN Fig. 1b. The BLUE IV category exhibited significant enrichment in 14 biological processes, with neuron development being the most significant ($P = 1.91 \times 10^{-4}$). On the contrary, the GRAY IV category exhibited significant enrichment in 3 biological processes, primarily related to cell-cell adhesion. Dysregulation in dietary intake[18,19] and insulin secretion[20] associated with neurotransmission can trigger the onset of type 2 diabetes (T2D), indicating that the BLUE category might exhibit correlated horizontal pleiotropy. Correlated horizontal pleiotropy, which is in the opposite direction of the actual causal effect, may be responsible for the failure of all methods to detect a significant causal relationship. We employed a bootstrap test to make causal inferences based on the GRAY category and obtained a near-significant result ($P_{gray} = 0.07, 95\%CL: (-0.022, 1.23)$).

SN 2 EM estimation

We apply the EM algorithm to estimate the parameters of $\widehat{\Theta} = \arg\max_{\Theta} \ln L(\theta)$, where

$$\ln L(\Theta) \propto \sum_i \sum_j \sum_k \left[Q\left(Z^{(i)} = (j,k)\right) \ln \frac{f\left(\widehat{\beta}_{Y,i} - \phi_j \widehat{\beta}_{X,i} - \theta_k | \phi_j, b_k\right) \cdot q_{\phi_j} \pi_{\theta_k}}{Q\left(Z^{(i)} = (j,k)\right)} \right]$$

To better illustrate the derivation of **the random effect model**, we first simplify by assuming two independent GWAS summary statistics of exposure and outcome, setting ρ to zero, and omitting the variance of exposure association $\hat{s}^2_{X,i}$, setting $\left(\phi_j\right)^2 \hat{s}^2_{X,i}$ to zero. Therefore, the distribution (4) in the main text,

$$\widehat{\beta}_{Y,i} - \phi_j \widehat{\beta}_{X,i} - \theta_k \sim N(0, \sigma^2)$$

where $\sigma^2 = \hat{s}^2_{Y,i} - 2\phi_j \cdot \rho \hat{s}_{X,i} \hat{s}_{Y,i} + \left(\phi_j\right)^2 \hat{s}^2_{X,i} + \beta^2_{X,i}\sigma^2_{\phi_j} + \sigma^2_{\theta_k}$, is simplified to

$$\widehat{\beta}_{Y,i} - \phi_j \widehat{\beta}_{X,i} - \theta_k | \phi_j, b_k \sim N\left(0, \hat{s}^2_{Y,i} + \widehat{\beta}^2_{X,i}\sigma^2_{\phi_j} + \sigma^2_{\theta_k}\right).$$

We set the initial parameters as $\Theta_0 = (q_{\phi_{j0}}, \phi_{j0}, \sigma_{\eta_{j0}}, \pi_{b_{k0}}, b_{k0}, \sigma_{b_{k0}})$, and let $\Theta_{old} = \Theta_0$.

In the E-step, we derive Q function by

$$Q\left(Z^{(i)} = (j,k) | \Theta_{old}\right) = \frac{f_{j,k}(\widehat{\beta}_{Y,i} - \phi_j \widehat{\beta}_{X,i} - \theta_k | \Theta_{old})}{\sum_j \sum_k p_{j,k} (\widehat{\beta}_{Y,i} - \phi_j \widehat{\beta}_{X,i} - \theta_k | \Theta_{old})}$$

where $f_{j,k}$ is the density function of $N(0, \hat{s}^2_{Y,i} + \widehat{\beta}^2_{X,i}\sigma^2_{\phi_j} + \sigma^2_{\theta_k})$.

In the M-step, we estimate parameters of interest to the maximum $\ln L(\Theta)$. By setting the derivative of $\ln L(\Theta)$ function to zero, we obtain:

$$\phi_j = \frac{\sum_i \sum_k \left[Q\left(Z^{(i)} = (j,k)\right) \widehat{\beta}_{X,i} \left(\widehat{\beta}_{Y,i} - b_k\right) \Big/ \left(\hat{s}^2_{Y,i} + \widehat{\beta}^2_{X,i}\sigma^2_{\phi_j} + \sigma^2_{\theta_k}\right) \right]}{\sum_i \sum_k \left[Q\left(Z^{(i)} = (j,k)\right) \widehat{\beta}^2_{X,i} \Big/ \left(\hat{s}^2_{Y,i} + \widehat{\beta}^2_{X,i}\sigma^2_{\phi_j} + \sigma^2_{\theta_k}\right) \right]}, \; j = 1, \cdots, n_\phi$$

$$b_k = \frac{\sum_i \sum_j \left[Q\left(Z^{(i)} = (j,k)\right) \left(\widehat{\beta}_{Y,i} - \phi_j \widehat{\beta}_{X,i}\right) \Big/ \left(\hat{s}^2_{Y,i} + \widehat{\beta}^2_{X,i}\sigma^2_{\phi_j} + \sigma^2_{\theta_k}\right) \right]}{\sum_i \sum_j \left[Q\left(Z^{(i)} = (j,k)\right) \Big/ \left(\hat{s}^2_{Y,i} + \widehat{\beta}^2_{X,i}\sigma^2_{\phi_j} + \sigma^2_{\theta_k}\right) \right]},\ k = 1, \cdots, n_\theta$$

$$q_{\eta_j} = \frac{\sum_i \sum_k Q\left(Z^{(i)} = (j,k)\right)}{\sum_i 1},\ j = 1, \cdots, n_\phi$$

$$\pi_{b_k} = \frac{\sum_i \sum_j Q\left(Z^{(i)} = (j,k)\right)}{\sum_i 1},\ k = 1, \cdots, n_\theta$$

The analytical solutions for $\frac{\partial L}{\partial(\sigma^2_{\phi_j})} = 0$ and $\frac{\partial L}{\partial(\sigma^2_{\theta_k})} = 0$ are complicated, so we use the optimization method to estimate:

$$\sigma^2_{\phi_j} = \arg\max_{\sigma^2_{\phi_j}} L(\Theta|\Theta_{old}),\ j = 1, \cdots, n_\phi$$

$$\sigma^2_{\theta_k} = \arg\max_{\sigma^2_{\theta_k}} L(\Theta|\Theta_{old}),\ k = 1, \cdots, n_\theta$$

Repeat the E-step and M-step until convergence. Just set $\sigma^2_{\phi_j}$ at zero, the derivation involves solving **the fixed effect model** of PCMR.

When considering the sample overlapping and not ignoring the variance of exposure, where $\rho \neq 0$ and $\left(\phi_j\right)^2 \hat{s}^2_{X,i} \neq 0$, the partial derivation of $\frac{\partial L}{\partial(\gamma+\eta_j)} = 0$ lacks an analytical solution. The estimation of ϕ_j also need by optimization method:

$$\phi_j = \arg\max_{\phi_j} L(\Theta|\Theta_{old}),\ j = 1, \cdots, n_\phi$$

We use the `optimize` function in R for the optimization method here.

SN 3 Alternative methods

We compare the performance of PCMR with six alternative methods, including IVW, Egger, Weighted-median, weighted mode, CAUSE and MRAID. We also compare PCMR's pleiotropy test with MR-PRESSO outlier test in detecting correlated horizontal pleiotropy. The candidate IVs are selected by each method default, and LD pruning ensures no pair of IVs has a pairwise $r^2 > 0.1$. These methods are implemented as follows.

method	R package	Version	Function	parameters	Threshold of IVs
IVW	MendelianRandomization	0.6.0	mr_ivw	default	5×10^{-8}
Egger	MendelianRandomization	0.6.0	mr_egger	default	5×10^{-8}
Weighted-median	MendelianRandomization	0.6.0	mr_median	default	5×10^{-8}
Median mode	MendelianRandomization	0.6.0	mr_mbe	default	5×10^{-8}
CAUSE	cause	1.2.0.0335	cause	default	1×10^{-3}
MRAID	MRAID	1.0	MRAID	default	5×10^{-8}
MR-PRESSO	MRPRESSO	1.0	mr_presso	default	5×10^{-8}

Note: MRAID can use a relaxed p-value threshold and estimate causal effect under LD, influencing the statistic power but not the false positive control.[21] For convenience, we use a strict threshold (5×10^{-8}) and LD pruning for MRAID.

References

1. Willer, C. J. *et al.* Discovery and refinement of loci associated with lipid levels. *Nat. Genet.* **45**, 1274–1283 (2013).
2. Yengo, L. *et al.* Meta-analysis of genome-wide association studies for height and body mass index in ~ 700000 individuals of European ancestry. *Hum. Mol. Genet.* **27**, 3641–3649 (2018).
3. Locke, A. E. *et al.* Genetic studies of body mass index yield new insights for obesity biology. *Nature* **518**, 197–206 (2015).
4. Lu, Y. *et al.* New loci for body fat percentage reveal link between adiposity and cardiometabolic disease risk. *Nat. Commun.* **7**, 10495 (2016).
5. Horikoshi, M. *et al.* Genome-wide associations for birth weight and correlations with adult disease. *Nature* **538**, 248–252 (2016).
6. Evangelou, E. *et al.* Genetic analysis of over 1 million people identifies 535 new loci associated with blood pressure traits. *Nat. Genet.* **50**, 1412–1425 (2018).
7. Dupuis, J. *et al.* New genetic loci implicated in fasting glucose homeostasis and their impact on type 2 diabetes risk. *Nat. Genet.* **42**, 105–116 (2010).
8. Liu, M. *et al.* Association studies of up to 1.2 million individuals yield new insights into the genetic etiology of tobacco and alcohol use. *Nat. Genet.* **51**, 237–244 (2019).
9. van der Harst, P. & Verweij, N. Identification of 64 Novel Genetic Loci Provides an Expanded View on the Genetic Architecture of Coronary Artery Disease. *Circ. Res.* **122**, 433–443 (2018).
10. Malik, R. *et al.* Multiancestry genome-wide association study of 520,000 subjects identifies 32 loci associated with stroke and stroke subtypes. *Nat. Genet.* **50**, 524–537 (2018).
11. Morris, A. P. *et al.* Large-scale association analysis provides insights into the genetic architecture and pathophysiology of type 2 diabetes. *Nat. Genet.* **44**, 981–990 (2012).
12. Demenais, F. *et al.* Multiancestry association study identifies new asthma risk loci that colocalize with immune-cell enhancer marks. *Nat. Genet.* **50**, 42–53 (2018).
13. Trubetskoy, V. *et al.* Mapping genomic loci implicates genes and synaptic biology in schizophrenia. *Nature* **604**, 502–508 (2022).
14. Howard, D. M. *et al.* Genome-wide meta-analysis of depression identifies 102 independent variants and highlights the importance of the prefrontal brain regions. *Nat. Neurosci.* **22**, 343–352 (2019).
15. Mullins, N. *et al.* Genome-wide association study of more than 40,000 bipolar disorder cases provides new insights into the underlying biology. *Nat. Genet.* **53**, 817–829 (2021).
16. Merino, J. *et al.* Genetically Driven Hyperglycemia Increases Risk of Coronary Artery Disease Separately From Type 2 Diabetes. *Diabetes Care* **40**, 687–693 (2017).
17. National Center for Chronic Disease Prevention and Health Promotion (US) Office on Smoking and Health. *The Health Consequences of Smoking—50 Years of Progress: A Report of the Surgeon General*. (Centers for Disease Control and Prevention (US), Atlanta (GA), 2014).
18. Wu, Q., Boyle, M. P. & Palmiter, R. D. Loss of GABAergic signaling by AgRP neurons to the parabrachial nucleus leads to starvation. *Cell* **137**, 1225–1234 (2009).
19. Krashes, M. J., Shah, B. P., Koda, S. & Lowell, B. B. Rapid versus delayed stimulation of feeding by the endogenously released AgRP neuron mediators GABA, NPY, and AgRP. *Cell Metab.* **18**, 588–595 (2013).
20. REV-ERB in GABAergic neurons controls diurnal hepatic insulin sensitivity - PubMed. https://pubmed.ncbi.nlm.nih.gov/33762728/.
21. Yuan, Z. *et al.* Likelihood-based Mendelian randomization analysis with automated instrument selection and horizontal pleiotropic modeling. *Sci. Adv.* **8**, eabl5744 (2022).